Earth, Planets and Space

FULL PAPER Open Access

Paleomagnetic constraint of the age and duration of the Taupō Eruption, New Zealand

Takeshi Hasegawa[1*], Annika Greve[2], Darren M. Gravley[3], Chie Kusu[1], Yasuaki Kaneda[1], Shohei Shibata[1], Makoto Okada[1], Szabolcs Kósik[4,5], Nobutatsu Mochizuki[6] and Gillian Turner[7]

Abstract

We have carried out paleomagnetic analyses of tephras from the Taupō eruption, one of the most violent eruptions on Earth in the past 5000 years. Pyroclastic deposits were collected with 7 cm^3 cubes pushed into each unit of the Taupō eruption sequence, consisting of airfall units and overlying ignimbrite. Where possible, we targeted fine-ash layers and matrix, as lapilli sized material can significantly affect the quality of the analysis. The samples were oriented using a collection device specially designed to maximize accuracy. All samples were subjected to alternating field demagnetization, while samples from Taupō ignimbrite (Y7)—the only unit deposited hot were also subjected to thermal demagnetization. The characteristic remanent magnetizations (ChRMs) for specimens from unit Y1, the lower and upper parts of unit Y4, and unit Y7 are well determined ($\alpha_{95} < 3.3°$). The declinations and inclinations of site-mean ChRMs range from 3.0° to 7.1° and − 53.4° to − 56.2°, respectively, in close agreement with published results from lithic fragments of the Taupō ignimbrite (Y7). The mean ChRM of unit Y3 does not fit within 95% confidence limits of the ChRM of other units. We presume this is a consequence of unit Y3 samples containing relatively coarse grains and of probable secondary process of the deposit. This outlier aside, our results show consistency between thermoremanent magnetizations of ignimbrite and detrital remanences of co-eval ashfalls, thus validating our method for further tephra research. Both geological observations and paleomagnetic estimation using angular difference suggest that the duration of the Taupō eruption sequence was less than a few tens of years. Furthermore, matching the overall mean ChRM direction (Dec = 4.3°, Inc = − 55.3°, $\alpha_{95} = 1.3°$, $N = 38$ specimens) to the New Zealand paleosecular variation record using the MATLAB dating tool, most likely supports a younger age (ca. 310 CE) than the reported wiggle match eruption age of 232 ± 10 CE.

Keywords Paleomagnetic dating, Duration of eruption, Taupō eruption, Tephra, Magnetization

*Correspondence:
Takeshi Hasegawa
takeshi.hasegawa.paul@vc.ibaraki.ac.jp
Full list of author information is available at the end of the article

Graphical Abstract

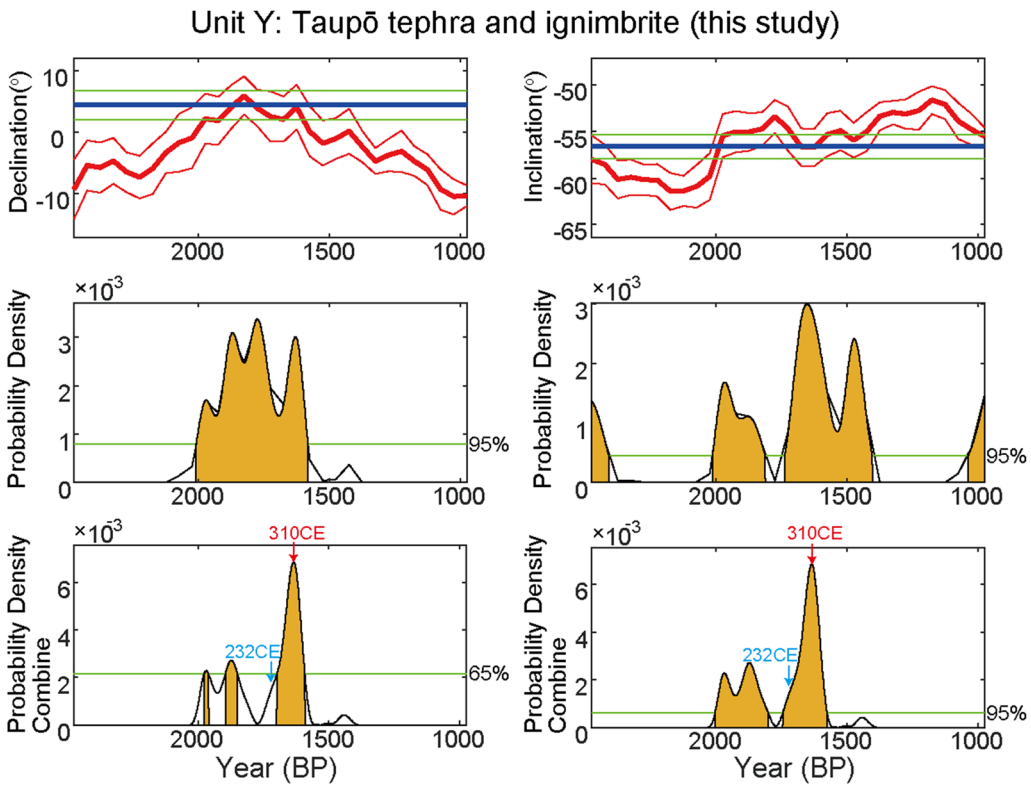

Introduction

Explosive eruptions, especially from silicic volcanoes, broadly disperse pyroclastic airfall materials that can provide key marker-beds in sedimentary sequences. For this reason, tephro-stratigraphic and -chronologic studies have been well developed in regions that have been subject to regular explosive rhyolitic volcanic activity through time, such as the Taupō Volcanic Zone (TVZ) in the North Island of New Zealand (e.g., Wilson et al 1984; Houghton et al. 1995). Volcanic rocks contain magnetic minerals, such as titanomagnetite and titanohematite that retain a remanent magnetization in the direction of the Earth's magnetic field during cooling and deposition. Correlation between the paleomagnetic information recorded by volcanic deposits with known records of secular variation can provide independent age estimates. This method has been used to produce high-resolution eruptive histories for volcanoes around the world (e.g., Böhnel et al. 2016; Pistolesi et al. 2021). While there are many studies of volcanic lava and welded ignimbrite deposits, only a few studies of volcanic airfall deposits have been published to date (e.g., Yukutake et al. 1964; Hayashida et al. 1996; Fujii et al. 2001; Hasegawa et al. 2018). This is likely due to the difficulties associated with collecting oriented samples for such materials. Considering the geomagnetic direction changes 0.05–0.20°/year, the dating method provides results with a time resolution of a few tens of years when the tephra site-mean ChRM direction is determined with a small α_{95} (e.g., less than 3°).

In this paper, we present the newly obtained results of paleomagnetic analyses for the Taupō eruption-one of the most violent eruptions worldwide in the past 5000 years. We determined the paleomagnetic directions from the Taupō eruption sequence (airfall and ignimbrite). We compared the paleomagnetic remanences recorded using differing processes (e.g., thermal vs. detrital) and discuss the advantages and limits of explosive eruption deposits for paleomagnetic dating. Paleomagnetic dating of tephra that has been deposited at relatively cool temperatures (i.e., airfall ash deposits) could provide a new method to constrain the age and duration of large eruptions, including those where tephra has been widely distributed across the globe.

Geological background: Taupō eruption

Eruption products and sequence

The first millennium Taupō eruption (unit Y) is the 27th eruption of Taupō volcano, following the caldera-forming Oruanui eruption at ~ 25.5 ka (Wilson 1993). The Taupō eruption is divisible into seven units (Y1–Y7 from Wilson 1993; note, however, we do not include the intra-plinian early ignimbrite Y6 flow units deposited synchronously with Y5 in our study) that occurred from multiple vent sites along a ~ 10 km-long fissure in the Horomatangi Reefs area of Lake Taupō (Fig. 1). The eruption sequence is globally recognized for its complexity of eruptive styles

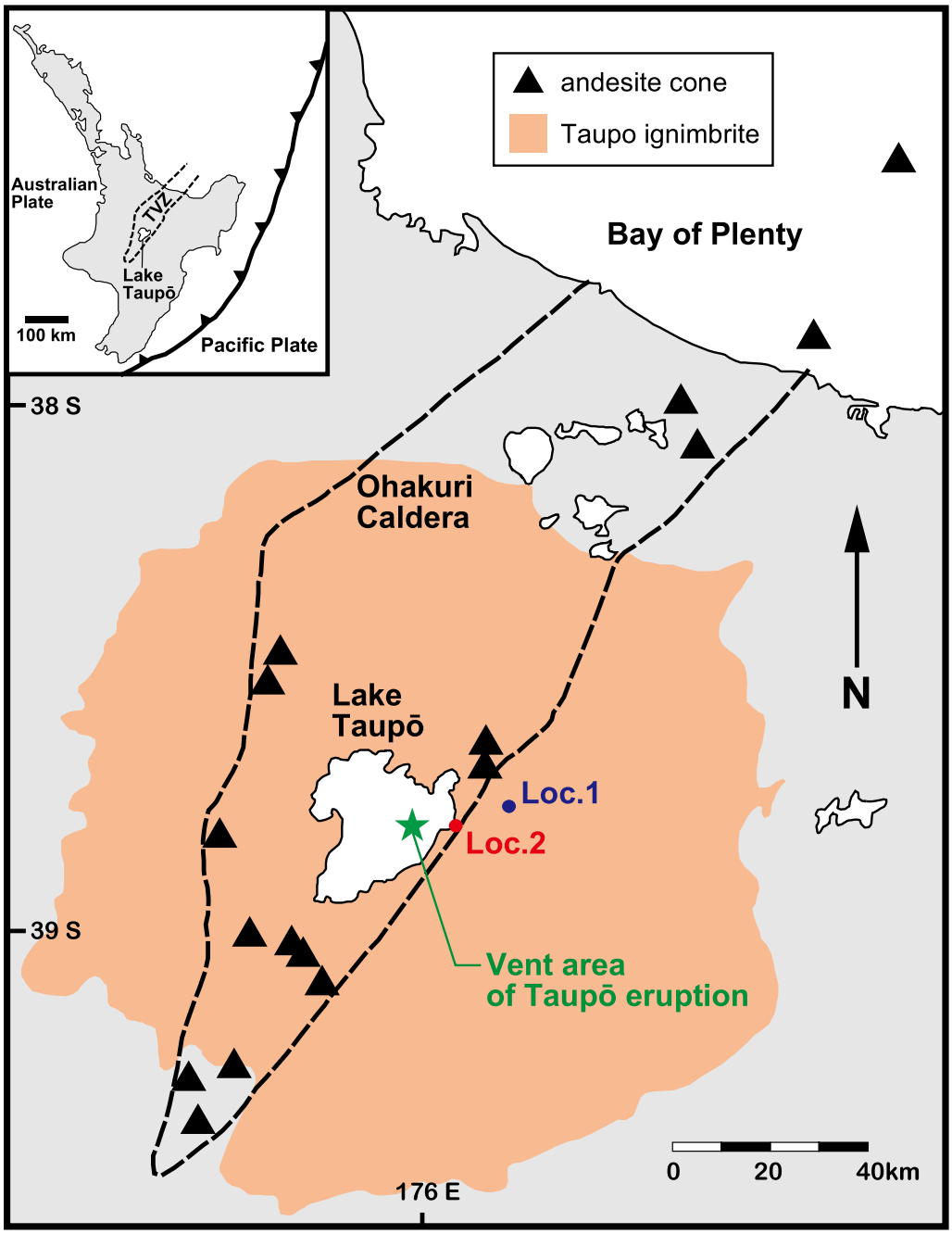

Fig. 1 Index map showing sampling locations (Loc.1 and 2) on Taupō Volcanic Zone (TVZ: dashed lines) with Lake Taupō. The outline of TVZ refers Houghton et al. (1995). Waterbodies (lakes and ocean) are shown by white pattern. The distribution of Taupō ignimbrite refers Wilson (1985). Colored map (www.topomap.co.nz) in yellow box is the close-up of sampling area

that is unrelated to its rather homogenous magma composition, but attributable to heterogeneities in magma volatile content, vesiculation and fragmentation depth, and extreme variations in magma and external water (lake) interaction (Wilson and Walker 1985; Smith and Houghton 1995a, b). Despite being downgraded from ultraplinian to plinian (see Houghton et al. 2014), phase 5 of the eruption sequence remains one of the most powerful eruptions worldwide in the past 5000 years with a maximum plume height of 35–40 km, and was followed by the climactic phase 7 which emplaced the Taupō ignimbrite.

We refer the reader to previously published studies for descriptions of the deposits from the seven eruption units (i.e., Walker 1980, 1981a, b, c; Wilson 1985; Wilson and Walker 1985; Smith and Houghton 1995a, b; Houghton et al. 2014). We focus here on the interpreted eruption style and emplacement mechanism for each unit (referred here as its associated 'eruption phase' and labeled in Fig. 2 as Y1 through Y7) and the duration of the eruption sequence based on published qualitative observations. The sequence began in the southwestern part of the fissure (vent 1 from Smith and Houghton 1995a) with a minor phreatomagmatic eruption that deposited the initial ash from a maximum plume height of 10 km (Wilson and Walker 1985). The relatively uniform nature and lack of subunits suggests this eruption phase may have lasted only hours (Wilson and Walker 1985). With little elapsed time, phase 2 of the eruption began from the same vent source with a significant increase in eruption rate that cleared the vent area of lake water and led to relatively continuous plinian activity and the vertical deposition of the coarse Hatepe plinian pumice over a period of 10–30 h (Wilson and Walker 1985). With no discernable time break, this plinian phase quickly transitioned into a phreatoplinian eruption (phase 3) as lake water accessed the vent and the Hatepe ash was deposited. Towards the end of this phase, widespread fluvially sourced (possibly related to the violently expelled lake water from the vent 1 source) erosion and gullying of the Hatepe ash took place and Wilson and Walker (1985) interpreted this to represent the longest time break in the entire Taupō eruption sequence, possibly several weeks. However, a subsequent high-resolution study of the phases 3 and 4 deposits by Smith and Houghton (1995a, b) demonstrated that while erosion was occurring at

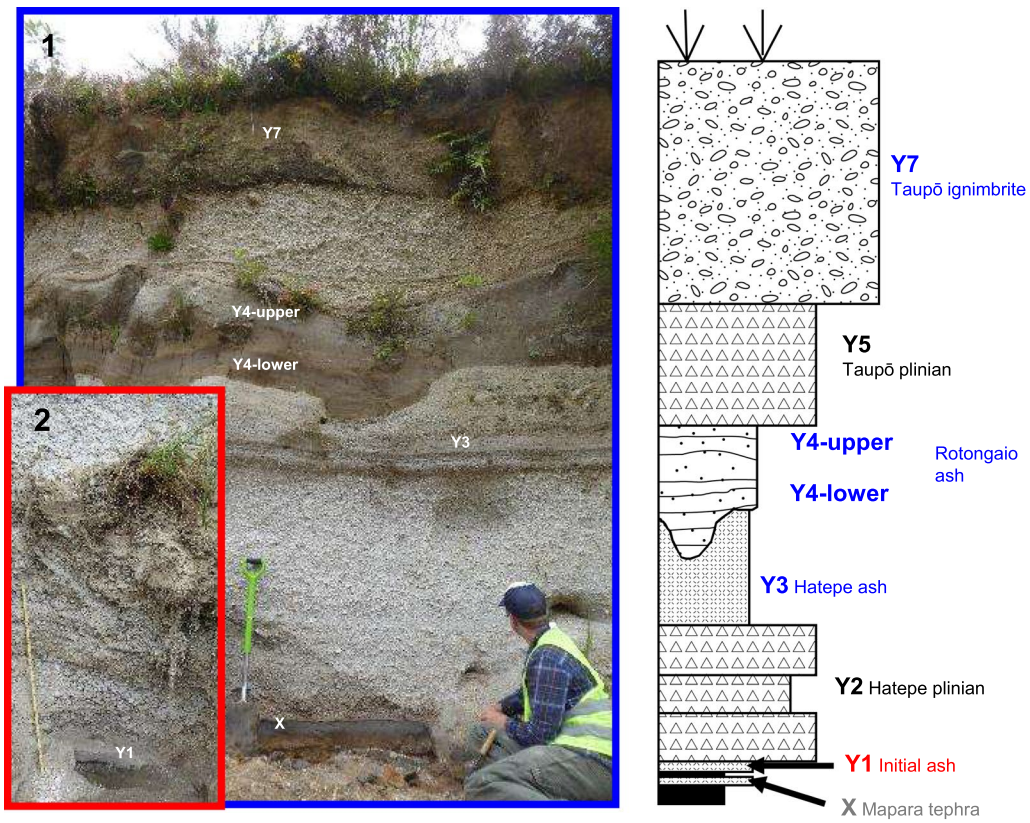

Fig. 2 Outcrop photo (left) and stratigraphic column (right) of Taupō eruption sequence. Unit name (and its abbreviations) are from Wilson (1993). Note that we do not include the intra-plinian early ignimbrite Y6 flow units deposited synchronously with Y5 in this study

the end of phase 3, there are interbedded Hatepe and Rotongaio (phase 4) ash deposits found northeast of Lake Taupō which demonstrate synchronicity between the phases as opposed to a discernable time break. Further, the character and distribution of the phases 3 and 4 deposits suggests that the Rotongaio magma was more degassed and erupted from a different source at the northeast end of the fissure (vent 2; Smith and Houghton 1995a). The Rotongaio ash is perhaps the most complex of the Taupō eruption deposits. It is predominately of phreatomagmatic origin but modes of emplacement vary within single beds from primary vertically driven ash fall to 'syneruptive slope-affected and fluvially reworked ash' (Smith and Houghton 1995b).

Following phase 4, an abrupt change from the wet erupted Rotongaio ash to the dry Taupō plinian pumice (phase 5) took place with another shift in vent position back to or in close proximity to the southwestern vent 1, location for phases 1, 2 and 3 (Houghton et al. 2014). The Taupō plinian pumice was deposited vertically from a powerful eruption plume that may have reached 40 km high. Walker (1980) suggested the mass discharge rate was sustained for up to 17 h, however, a relatively recent study (Houghton et al. 2014) identified 26 subunits within the phase 5 deposits at 149 field locations and demonstrated that the mass discharge rate waxed and waned with corresponding changes in plume height through its duration. Phase 5 did include some laterally emplaced flow deposits (Y6 from Wilson 1993) likely related to intermittent column collapse (Wilson and Walker 1985), but these flow units pale in comparison to the magnitude of the phase 7 Taupō ignimbrite. The transition from phase 5 to phase 7 was accompanied by a significant increase in magma eruption rate of up to two orders of magnitude. Thus, the Taupō ignimbrite was not simply the effect of column collapse from the phase 5 eruption plume, but more a blast directed in every direction from the vent (Wilson 1985). The entire ignimbrite was emplaced, up to 90 km from the vent source, in approximately 400 s and at speeds of up to 250–300 m s^{-1} (Wilson 1985).

In summary, from calculated eruption rates for each phase of the eruption, combined with evidence for non-volcanic erosion of deposits within the sequence, Wilson and Walker (1985) estimate a total duration for the Taupō eruption to be a maximum of weeks to months. This more qualitative geologic evidence (i.e., field observations of the deposits) suggests that there were no significant time breaks within the eruption on the order of years to decades. The eruption was extraordinarily complex with a combination of fall and flow deposits from variably wet to dry eruption plumes, and intermittent hybrid vertical to lateral transport that included syn-eruption water-laden currents during phase 4. The emplacement temperatures of the deposits, thus, varied widely from relatively cold deposition from wet plumes or powerful high and dry eruption columns, and hot emplacement from the more directed currents associated with the phase 7 Taupō ignimbrite (cf. paleomagnetically derived temperatures from McClelland et al. 2004).

Eruption age

The Taupō ignimbrite (Y7) contains abundant organic materials such as charcoal and carbonised logs, and has been dated multiple times by ^{14}C methods (Hogg et al. 2019 and references therein). However, diversity of sample species and dating methodology has resulted in a dispersion of dates ranging nearly 200 years from 130 to 320 CE (Lowe and de Lange 2000; Hogg et al. 2019). The suite of contiguous decadal ^{14}C dates from the tanakeha (*Phyllocladus trichomanoides*) log in Y7 was statistically wiggle-matched against the kauri (*Agathis australis*) calibration curve for New Zealand to derive a more precise calendar date of 232 ± 10 CE (95% probability range) (Hogg et al. 2012). After that, the date has been challenged on the basis of potential magmatic carbon dioxide contamination of the radiocarbon measurements (Holdaway et al. 2018). Holdaway et al. (2018) concluded that the Taupō eruption occurred decades to possibly two centuries later than 232 CE, but the possibility was refuted by Hogg et al. (2019) and is still controversial (Holdaway et al. 2019). The most recent review by Lowe and Pittari (2021) concurs with the wiggle-matched eruption date of 232 ± 10 CE.

Samples

We sampled the entire Taupō eruption sequence at a well-known type locality on State Hwy 5 (Loc.1: S38°44′51″, E176°11′59″), with the exception of the phase 1 (initial ash) deposit which was too thin to sample at this location (see Fig. 1 for the two locations). We refer to the Taupō eruption stratigraphy using Wilson's (1993) unit Y designation followed by the eruption phase (see Fig. 2). Paleomagnetic samples were collected by pushing 7 cc plastic or aluminum cubes into fine ash layers of each phase in the stratigraphy (Figs. 2, 3), as lapilli sized material within the cube significantly affects the quality of the analysis. Thus, the Hatepe plinian (Y2) and Taupō plinian (Y5) deposits, which contain coarse pumice, could not be sampled. Although samples were carefully taken from the finer (matrix) part of Hatepe ash (Y3) and Taupō ignimbrite (Y7), it was difficult to avoid lapilli-sized grains in their cubes (see below for detail). Because of the complexity in the interpreted mode of deposition (vertical ash fall vs. lateral emplacement with flushed lake water) of the Rotongaio ash (Y4), sampling

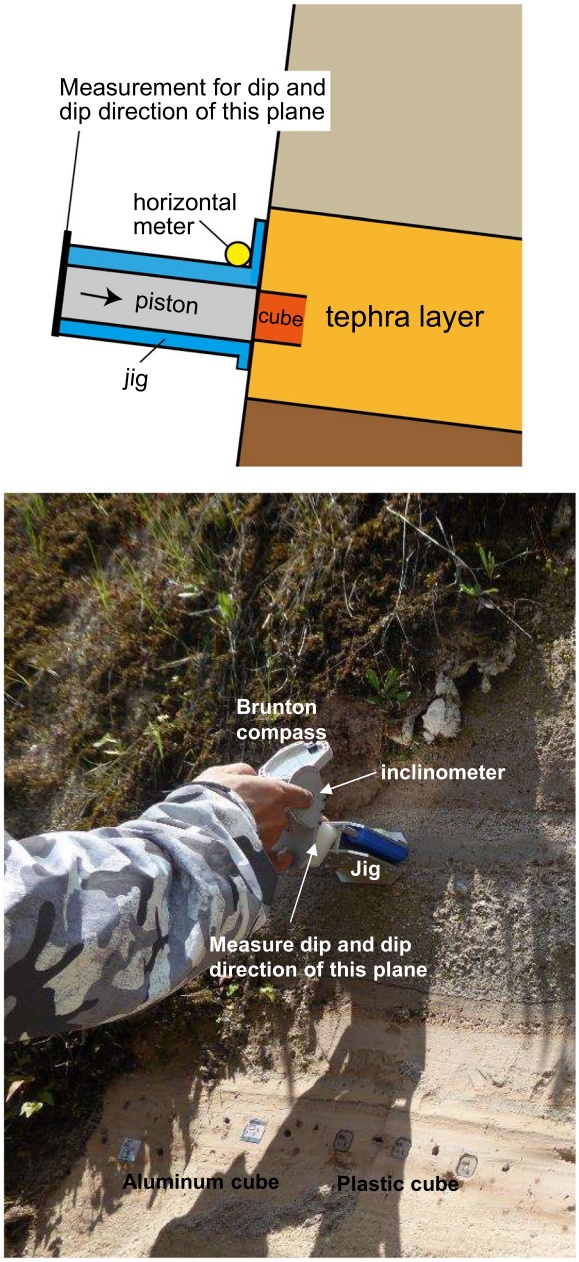

Fig. 3 Schematic illustration (upper) and photograph (lower) for oriented sampling for tephra layers

levels were further divided into the Y4-lower and -upper parts of the deposit. As mentioned above, only Y1 was sampled at a different and more proximal location (Loc.2: S38°48′03″, E176°04′38″) to its source vent. To obtain reference data for comparison with the Taupō eruption data, we sampled unit X (Mapara tephra: Wilson 1993), which underlies Y1 and an intervening thin soil at Loc.1. Prior to removal from the outcrop, the samples were oriented using an orientation device with magnetic compass (and sun compass) and inclinometer that were integrated in a specifically designed (Natsuhara-Giken) (Fig. 3). For details of the sampling procedures, refer to Mochizuki et al. (in prep). During this process, the measured azimuth was corrected for the local declination of 21° East (ref: International Geomagnetic Reference Field (IGRF-13): https://wdc.kugi.kyoto-u.ac.jp/igrf/index-j.html). To check for within-site variations and, whether there were differences within individual phases of the eruption sequence, at least eight samples (cubes) were collected (within 10 m lateral extent) and mean directions calculated for each phase (and sometimes separate sub-units within a phase, i.e., the upper and lower parts of Y4).

Paleo- and rock magnetic methods

Magnetic analyses included (in the following order) measurement of the anisotropy of magnetic susceptibility (AMS), natural remanent magnetization prior to and following progressive alternating field—(AFD) or thermal demagnetization (THD). AMS measurements were conducted using an AGICO Kappabridge KLY-3 at Ibaraki University (IU), with the aim of constraining pyroclastic transport mechanisms and directions. Most samples were subsequently subjected to stepwise AFD using an AGICO LDA-5 AF demagnetizer (at IU) to a peak alternating field of 130 mT. Remanences were measured by a AGICO JR-6A at IU. THD was conducted on samples from unit Y7, which was assumed to be the only unit deposited hot, using a TD-48, ASC Scientific furnace (at IU) up to a peak temperature of 630 °C. Characteristic remanent magnetization directions (ChRM) were calculated using principal component analysis (PCA) (Kirschvink 1980). Datapoints for ChRM calculation were selected from the most stable component towards the origin of the vector component plot. As a result, the maximum angular deviations (MAD) for Y1, Y4 and unit X was less than 3°. Demagnetization plots for samples of deposits Y3 and Y7 display a larger dispersion and data from samples for which the principal component analysis returned MAD values exceeding 10° were rejected (Additional file 1: Table S1). Unit (site) mean directions and 95% confidence intervals were calculated from individual specimen ChRM directions using Fisher statistics (Fisher 1953).

Thermomagnetic analyses were also carried out on representative chip (approximately 3 g each) samples from the Y3, Y4-upper and Y7 units using a NMB-89 Natsuhara Giken magnetic balance at Kochi University. These analyses included heating of samples to a peak temperature of 700 °C with a rate of 10 °C/min. For comparison, thermomagnetic experiments were conducted either in vacuum (1–10 Pa) or in ambient atmosphere.

After the paleomagnetic analyses, we performed grain size analysis of samples to evaluate the effect of lapilli sized materials on the quality of paleomagnetic analyses. Samples from each cube were firstly dried and sieved at 1 ϕ intervals in the range −5 to 4 ϕ ($\phi = -\log_2 D$, where D is the particle diameter in millimeters). Secondly, finer fractions (< 63 μm = 4 ϕ) were analyzed by a laser scattering particle size analyzer (HORIBA LA-300). These data were combined and calculated to determine median (Md_ϕ) and sorting (σ_ϕ) based on Folk and Ward (1957).

Previous paleomagnetic research: emplacement temperature estimation on lithic fragments of the Taupō ignimbrite deposit

McClelland et al. (2004) report paleomagnetic directions for the Taupō ignimbrite deposit (Y7) from 44 sites that are distributed throughout the Central North Island. The study was conducted prior to the availability of continuous secular variation records or models. It was pursued with the aim to reconstruct emplacement temperature on ignimbrite clast deposits with distance from the vent.

In non-welded ignimbrite deposits, where the absence of a temperature indicator inhibits estimation of emplacement temperatures, thermal demagnetization techniques can be a powerful tool to estimate heating or deposition temperatures that are lower than the Curie temperature (T_c) of the predominant remanence carrier. In a sample with a mixed assemblage of magnetic grains with differing grain-size and blocking temperature distribution, we assume that only those grains that yield a blocking temperature lower than the emplacement temperate record a stable coherent magnetization that yields a characteristic remanent magnetization (ChRM) direction parallel to the ambient magnetic field at the time of emplacement. If the emplacement temperature exceeds T_c, and no secondary chemical remanent magnetization (CRM) or viscous remanent magnetization (VRM) was acquired after the initial remanent acquisition, a sample would display a single component ChRM.

McClelland et al. (2004) sampled and thermally demagnetized 488 samples from lithic clasts and 123 samples from pumice, which were collected in roughly vertical profiles through the deposit. While the study on pumice clasts was inconclusive, the lithic clasts showed a positive correlation between inferred emplacement temperature and distance from the vent. Clasts sampled within a 40 km radius from the vent recorded remanence directions that are roughly parallel to the present-day field, up to peak blocking temperatures between 150 and 300 °C. In contrast, the emplacement temperatures estimated from clasts that were sampled further afield range from 400 to 500 °C and show random remanence directions. Figure 4 displays

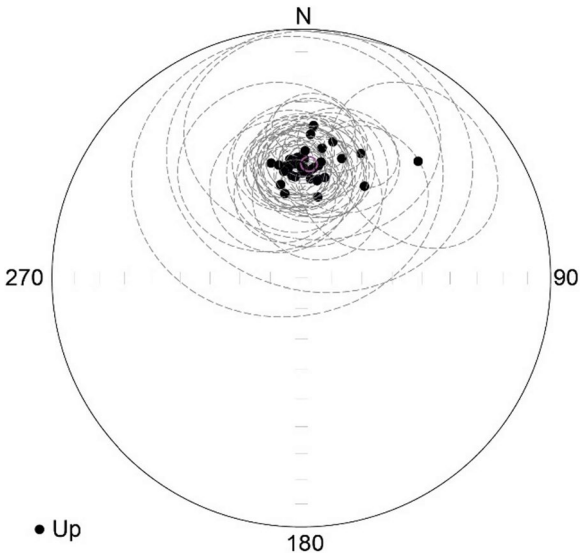

Fig. 4 Stereographic projections displaying the site mean directions (negative inclinations, black dots) and corresponding 95% confidence cones (dashed lines) of the low T_b components for lithic fragments in Taupō ignimbrite (Y7) reported in McClelland et al. (2004). The mean direction (pink circle) was calculated using Fisher statistics from the all site mean directions ($N = 44$)

Table 1 Mean directions for each unit

Unit	*N*	Dec	Inc	α_{95}	*k*
Y7	15	3.0	−55.8	2.5	237.2
Y4-upper	7	4.4	−55.4	3.3	328.2
Y4-lower	8	7.1	−56.2	1.7	1102.9
Y3	9	338.9	−56.8	5.8	78.9
Y1	8	3.9	−53.4	2.7	426.8
Y1, Y4, Y7 (overall mean)	38	4.3	−55.3	1.3	335.6
Y7 (lithic fragments)[a]	44[b]	3.9	−52.2	2.4	74.6[c]
X (Mapara tephra)	9	358.8	−54.3	2.9	2.9

[a] Data from McClelland et al. (2004) and calculated by Greve and Turner (2017)

[b] Number of individual site mean directions

[c] Calculated by this study

the site mean directions and 95% confidence intervals reported for the low T_b components. Reported site mean directions mostly overlap at the 95% confidence level. Declinations range from −12.5° to 45.1° and inclinations from −34.1° to −62.9°. The angle of 95% confidence (α_{95}) ranges from moderate values of 5.9° up to 49.6° (Fig. 4). Greve and Turner (2017) calculated a unit mean direction for the Taupō Ignimbrite from the reliable site mean low T_b components of McClelland et al. (2004): Dec = 3.9°, Inc = −52.2°, $\alpha_{95} = 2.4°$, $N = 44$ sites (Table 1).

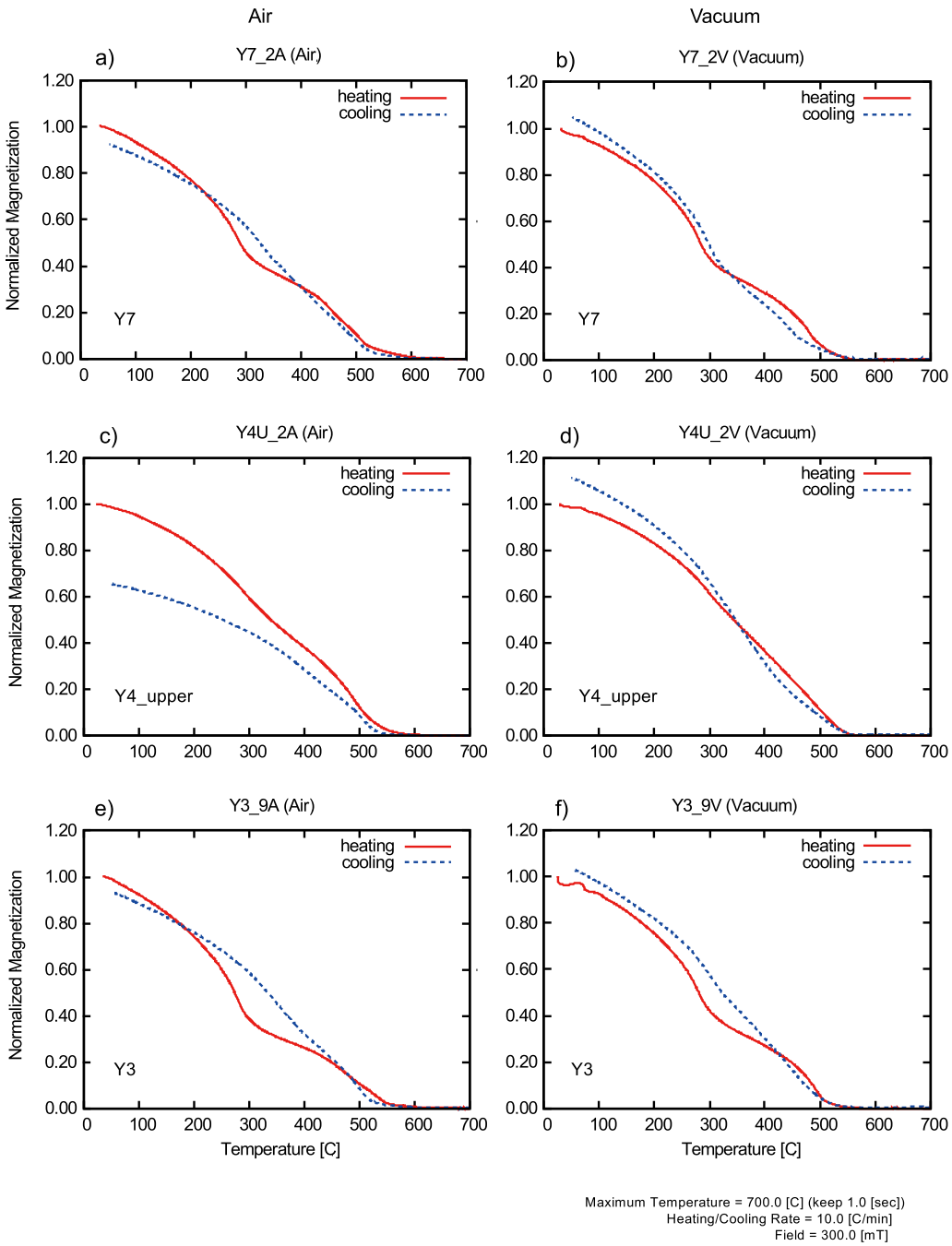

Fig. 5 Rock-magnetic properties (thermomagnetic curves) of selected samples. The vertical axis is the magnetization (MS) in an applied field of 0.2–0.3 T, which is normalized to that at 100 °C (MS0). Red and blue lines indicate heating and cooling curves, respectively

Results

Thermomagnetic analysis

Thermomagnetic curves usually display two distinct changes in slope between 250 and 300°C, and between 540 and 600 °C (Fig. 5). The latter coincides with the Curie temperature (T_c) of titanium-poor titanomagnetite—pure magnetite, while the first could indicate the T_c of a titanium-poor titanomagnetite. The cooling curves are mostly reversible, although a slight shift in the saturation magnetization and inversion points is visible in most diagrams. These shifts are likely the result of the decomposition of titanomaghemite to magnetite/hematite and/or oxy-exsolution of titanomagnetite/titanohematite solid solution series (see, for example, de Groot et al

2014; Greve and Turner 2017). The mineral alteration appears to be enhanced during thermomagnetic experiments conducted in an ambient atmosphere, as seen in particular in a decrease of the saturation magnetization measured in the cooling curve of sample Y4-upper (Fig. 5c), indicative of the oxidation of the original magnetic mineral phases.

Demagnetization behavior

During alternating field and thermal demagnetization, almost all samples show a single stable component of magnetization with little variability observed between individual units. The NRM intensities range from 3.5×10^{-2} to 5.4×10^{-1} A/m. During AFD samples lose ca. 90% of their remanence intensity at applied peak fields lower than 60 mT, with median destructive fields (MDF) around 30 mT (Fig. 6b–f). Samples from depositional unit Y3 display a larger data scatter and ChRM directions for Y3 yield maximum angular deviations (MAD) mostly above 6° (maximum: 13.9°) (Fig. 6e, Additional file 1: Table S1). During THD, magnetizations decrease linearly towards the origin of the vector component plot in the blocking temperature interval 0–480 °C, after which they retain 10% or less of the NRM. Evidence for multiple-components of magnetization, as would be expected if the samples were emplaced at a temperature lower than the peak blocking temperature measured here, is not recognized for the samples of Y7. Data from just two samples, Y3_2 and Y7_7, with MADs above 10° were removed from the mean direction calculations. The mean directions for each unit were calculated from ChRM directions for 47 samples (Table 1).

Mean directions

Table 1 and Fig. 7 summarize unit mean ChRM directions and 95% confidence limits for all units sampled. Assuming that the ChRM directions for each cube specimen in each unit are statistically independent of each other, we calculated a mean direction for each unit (Y1–Y7). The ChRM directions for specimens from units Y1, Y4-lower, Y4-upper and Y7 are well grouped with α_{95} values of 3.3° or less. The mean directions for these units range in declination from 3.0° to 7.1°, and in inclination from −53.4 to −56.2° and are not distinct at the 95% confidence limit (Table 1; Fig. 7). Y1 was sampled at a different location from the other units (Fig. 1), and the consistency of its and the other ChRM directions indicates that the data were not influenced by local effects such as tectonic block rotation or tilting. The mean direction of unit Y3 is less well defined. Y3, for which demagnetization data also is of lower quality, displays a NW—N elongated distribution of ChRM directions (Fig. 7). The Fisher (1953) precision parameter (k) of unit Y3 is considerably lower (78.9)

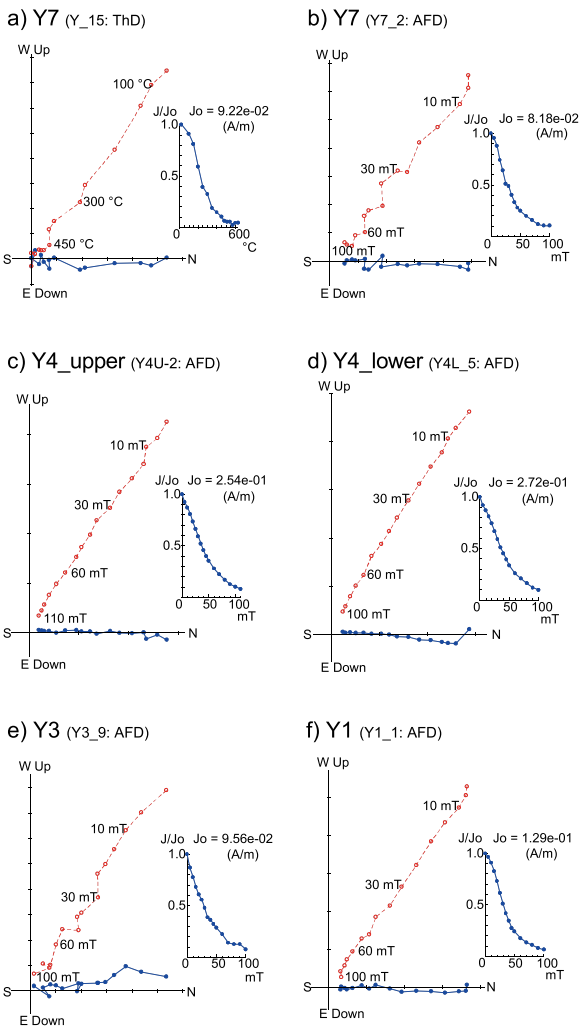

Fig. 6 Representative orthogonal vector plots for NRM of the measured samples. AFD: alternating field demagnetization, ThD: thermal demagnetization. Blue and Red plots are projections onto horizontal and vertical planes, respectively

than those of other units (>237.2). The best mean of Y3 (Dec = 338.9°, Inc = −56.8°, α_{95} = 5.8°) does not overlap with the 95% confidence limits of other Taupō eruption units.

The mean ChRM direction of unit X has Dec = 358.4°; Inc = −54.7°; α_{95} = 3.2°; N = 9 samples (Table 1). This direction is distinct from those of Taupō eruption units, particularly in declination.

AMS

Anisotropy of magnetic susceptibility (AMS) measures the alignment of paramagnetic- and ferrimagnetic mineral grains in a sample. During the terminal stages of fluvial transport, grains tend to align with their long axes in the transport direction, while later compaction by

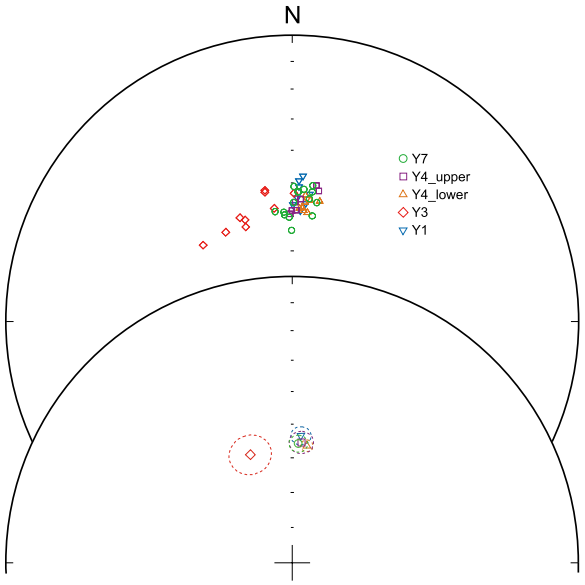

Fig. 7 Plots of mean directions for each unit

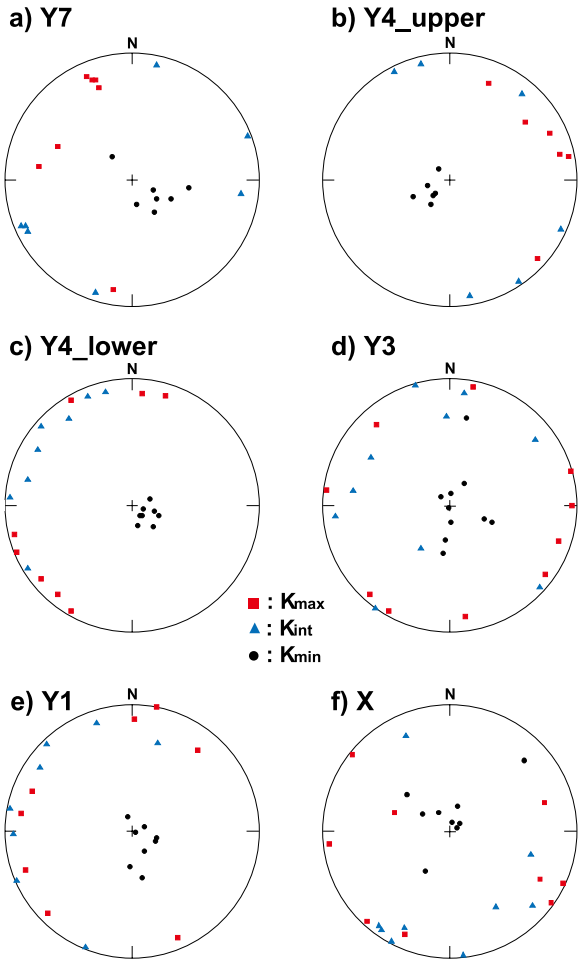

Fig. 8 Lower-hemisphere stereographic projections of the principal axes of magnetic susceptibility (AMS) for each unit. Black: K_{max}, Blue: K_{int}, Red: K_{min}

overburden loading may result in the alignment of minerals in the horizontal plane (e.g., MacDonald and Palmer 1990; Fisher et al. 1993; Baer et al. 1997). We use AMS data to distinguish and characterize different emplacement modes, such as airfall, and/or flow deposits and to identify sediment imbrication. AMS measures the bulk fabric of a sample, in typical minerals that often contribute, the maximum (K_{max}) and minimum (K_{min}) susceptibility axes are aligned with the longest and shortest grain axes, respectively (e.g., Hamilton and Rees 1970; Taira and Scholle 1979; Tarling and Hrouda 1993; Borradaile et al. 1999).

Figure 8 shows the distribution of the three principal axes of magnetic susceptibility in an equal-area projection. Statistical parameters of Jelinek (1981) such as magnetic foliation (F), magnetic lineation (L) and P' (corrected degree of anisotropy), T (shape parameter), q (shape factor) are shown in Additional file 1: Table S1. All units show almost vertically clustered K_{min} directions, although some of them are slightly offset. K_{max} of Y1 and Y3 (+unit X) are randomly distributed in the horizontal plane, while those of other units are more or less biased, probably reflecting flow or topographic effects.

Grain-size

Grain-size analyses showed that samples from deposits of Y3 and Y7 are relatively coarse ($Md_{\phi} = 2.38$ and 1.99, respectively) (Fig. 9a). Sample cubes of Y1 and Y4 were free of lapilli sized ($< -1\ \phi$) grains, whereas Y3 and Y7 contained considerable amounts (>10 wt%) of lapilli-sized grains (Fig. 9a). One cube of Y3 included a large pumice fragment, 8 mm in diameter. In the field, Y3 (Hatepe ash) has a moderately sorted lithofacies composed of fine ash with a scattering of pumice lapilli. Although, we carefully selected the fine ash part of Y3 and Y7 for sampling, the cubes contained lots of lapilli-sized materials.

The sorting indices for Y3 and Y7 are also poorer ($\sigma_{\phi} = 2.92$ and 2.30, respectively) than those of the other deposits. Grain-size histograms of Y3 and Y7 show flat distributions suggesting lateral flow transportation. That is consistent with the geological observation of Y7 that is interpreted as ignimbrite. Units Y1 and Y4 show clearer unimodal peaks, around 2–5 ϕ resulting in a relatively well sorted index ($\sigma_{\phi} = 1.73$–2.32), and are geologically interpreted as vertically emplaced airfall units. Details will be discussed with AMS data in the next section.

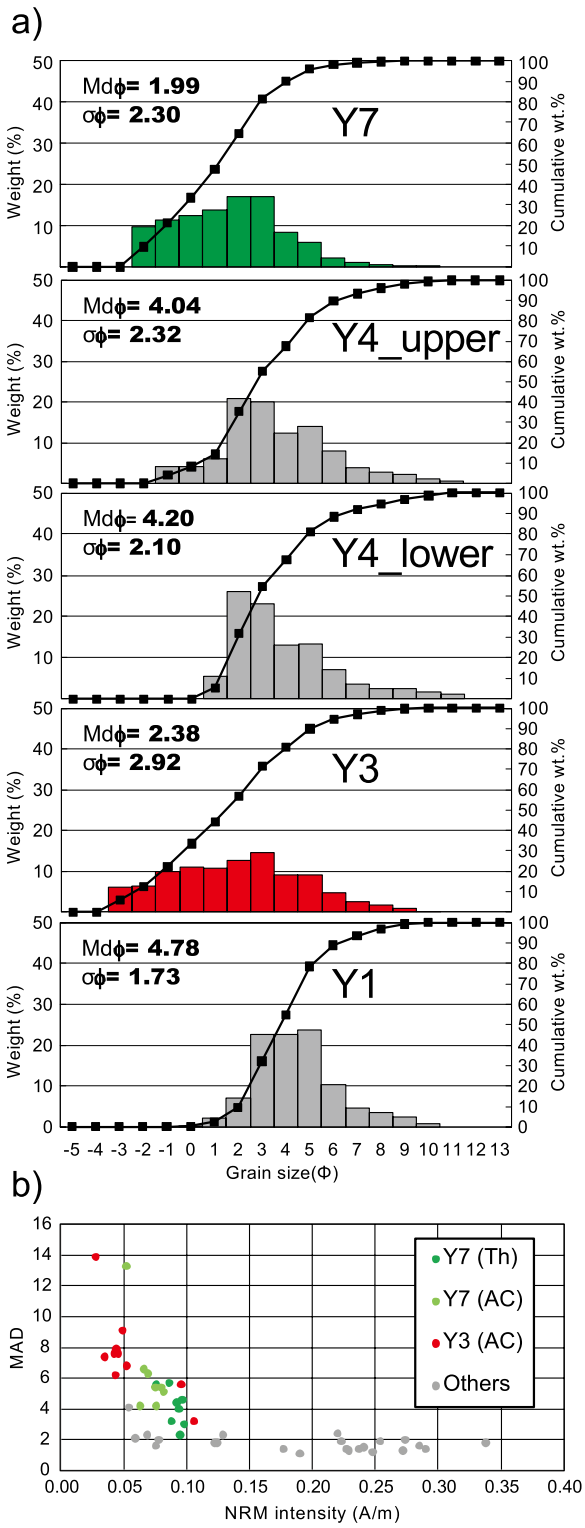

Fig. 9 Diagrams showing **a** grain size distribution histogram of each unit and **b** relationship between MAD and NRM. Note that cubes of Y3 and Y7 are rich in coarser grains

Discussion

Evaluation of the paleomagnetic data, magnetization and emplacement processes

ChRM directions of samples from deposits Y1, Y4-lower, Y4-upper and Y7 show an overall good agreement and their best unit-mean directions overlap at the 95% confidence level (Fig. 7). However, the mean direction of deposit Y3 is distinct from that of the other deposits. The larger MAD values recorded during demagnetization of samples from this deposit and the broader data distribution ($\alpha_{95}=5.8°$) suggest that samples from this site do not carry a coherent detrital or thermal record of the field at the time of deposition. We consider it unlikely that samples of these deposits are affected by more severe secondary remagnetization through weathering than the samples from other deposits in the same outcrop. Instead, it is possible that coarse fragments in these deposits resisted magnetic alignment during deposition and so do not contribute to the detrital remanence in the same way as the finer particles. Furthermore, the oval distribution of the individual ChRM directions could be indicative of a re-alignment of the grain assemblage, which could for example have been caused by basal dragging in a SW direction beneath overlying deposits. This mechanism may also explain the overall lower remanence intensities recorded. In contrast to samples from Y3 which were emplaced cold, samples from Y7, which was also poorly sorted but emplaced at high temperature and so carry a TRM, display ChRM directions that are coherent with all other deposits (Fig. 7, Additional file 1: Table S1).

Assuming that deposits Y1, Y4 and Y7 were emplaced and magnetized over a short time-period during which negligible secular variation occurred, we estimate a best mean ChRM direction from all samples from these units: Dec = 4.3°; Inc = −55.3°; $\alpha_{95}=1.3°$; $N=38$ samples (Table 1). This mean direction is almost consistent with the published mean calculated for lithic fragments emplaced within the Taupō ignimbrite (Y7) (McClelland et al. 2004; Greve and Turner 2017, refer to "Previous paleomagnetic research: emplacement temperature estimation on lithic fragments of the Taupō ignimbrite deposit" section), although the inclination is slightly shallower than our data (Table 1).

We can also use the AMS data to suggest the mode of emplacement of each unit. In the case of ignimbrites, K_{max} is expected to parallel the flow direction due to aerodynamic effects, and K_{min} is expected to be slightly tipped back from vertical against the flow due to imbrication (Baer et al. 1997; Ort et al. 2003). For example, in Y7,

the K_{max} axes fall in the western side, while K_{min} displays imbrication in an eastern orientation typical for strong flow in W–E direction. As the vent is located to the west of the sampling site, this finding is consistent with a transport of the ignimbrite from the vent to the sampling location along topographic low. On the other hand, in units Y1 and Y3 (+unit X), K_{max} are distributed around the horizontal plane with K_{min} vertical, which is typical for an airfall deposit, where gravitational loading resulted in the compaction and alignment of mineral grains in the horizontal. However, while the magnetic shape ellipsoids of unit Y1 (+unit X) are oblate ($T>0$), Y3 displays T values around 0 (−0.78 to 0.38) and high Q values (>0.67) which suggest that the deposition was not only controlled by vertical loading but also some secondary process (e.g., aforementioned dragging).

Y4-lower and Y4-upper might have been deposited as airfall on a slightly sloping surface on the eroded top of Y3 (cf. Smith and Houghton 1995b). Y4-lower displays a planar AMS structure that is dipping 10° to the NW without a clear imbrication. A possible explanation for this fabric could be a fall deposit on a dipping slope. Y4-upper also has a planar AMS structure dipping slightly to the NE suggesting deposition on a gentle slope.

Comparison between airfall and ignimbrite: mechanisms of remanence acquisition

In this study, we recognized agreement of ChRM directions between the ignimbrite unit (Y7) and preceding airfall units (Y1 and Y4). Consistency between thermoremanent magnetizations recorded by hot ignimbrite deposits and the detrital remanences of their co-eval ash/fall deposits have been described in a few previous studies (Reynolds 1979; Hayashida et al. 1996; Fujii et al.; 2001). However, there is no detailed study to investigate the magnetization processes of airfall deposits. Hasegawa et al. (2020) sampled and determined ChRM directions for several pumice clasts in a proximal airfall deposit, Osumi pumice fall (OPF) that preceded the 30 ka Ito ignimbrite, southern Kyushu. All pumice clasts in OPF show unblocking temperatures above 500 °C and the same ChRM directions suggesting the deposit was emplaced in hot (>500 °C) conditions resulting in thermoremanent magnetization (Hasegawa et al. 2020). However, this is a special case of a very proximal airfall deposit. Y1 and Y4 in this study comprise very fine ash and our sampling site is 20 km from the source. The distance from source and the phreatomagmatic nature of the eruptions that produced Y1 and Y4 (cf. Smith and Houghton 1995a) suggest these airfall units must have been cold enough to exclude the possibility of a primary thermoremanent. The possibility of partial remagnetization by the subsequent hot emplacement of the overlying Taupō ignimbrite can also be excluded. A conductive cooling model can be used to estimate the maximum temperatures reached in unit Y4 as a result of emplacement of the Taupō ignimbrite, Y7. The model of Lerner et al. (2019) employs dimensionless depth, time and temperature variables, making it straightforward to substitute appropriate values for particular situations. Assuming a 2 m thick ignimbrite with a uniform initial temperature of 400 °C (McClelland et al. 2004), ambient and initial temperature of the in-place tephra of 20 °C, and thermal diffusivities of 4.33×10^{-7} m^2/s for both ignimbrite and tephra (calculated from values given by Keating (2005) in modelling Mount St. Helens ignimbrite and non-welded tephra), we estimate that the top of unit Y4, ~1 m below the ignimbrite contact, reached a maximum of ~100 °C about 30 days after emplacement, while the base of Y4, 1 m deeper, reached a maximum of ~60 °C about 60 days after emplacement (Additional file 2: Fig. S1). At these depths the temperature profile changes only slowly, and so these temperatures, though low, would have remained elevated for weeks to months, making a low unblocking temperature viscous remanent magnetization possible. This simple model, however, takes no account of initial non-uniformity or the possible cooling effect of water percolating through the ignimbrite and/or substrate, which would lower the maximum temperature estimates (Keating 2005). Thermal or viscous remanent magnetization or remagnetization are, therefore, unlikely to affect more than the lowest unblocking temperature grains (≤100 °C) of the airfall units.

We infer that a process of depositional remanent magnetization works for fine grained airfall units such as Y1 and Y4, as discussed by Yukutake et al. (1964) at Izu Oshima Volcano. Pyroclastic materials are normally rich in magnetic minerals such as titanomagnetite. In particular, fine components are affected by magnetostatic forces that orient the magnetized axis with the geomagnetic field, while slowly falling through the air and settling. Even where coarse particles are contained, and may not be aligned to the direction of the magnetic field (as in Y3 cubes), the bulk deposits can be magnetized in the direction during the sedimentation processes. In the case of depositional remanent magnetization, inclination shallowing is sometimes observed in sedimentary rocks. However, the remanent magnetization directions of units Y1 and Y4 in this study show no shallower inclinations compared with that of the overlying ignimbrite (Y7).

As has been emphasized, the mean ChRM directions of airfall units (Y1 and Y4) agree well with that of ignimbrite unit (Y7). This is indicative of almost coeval timing of the thermal and depositional magnetizations just after the eruption. Considering the cooling rate of the ignimbrite (e.g., Kamata et al. 1993), the depositional

remanent magnetization of the airfall occurred within a short period of time—a few years or less. More field and experimental observations are necessary, but from our data, the depositional remanent magnetization associated with magnetized particles in airfall deposits appears to be locked soon after deposition.

Paleomagnetic control of the duration of Taupō eruption

We attempt to quantitatively estimate the duration of the Taupō eruption on the basis of obtained paleomagnetic directions and the rate of change of the NZPSV10k secular variation curve. Recent paleomagnetic studies reported that eruption durations of some large scale (VEI = 6 or more) eruptions were longer than previously thought; possibly tens to a hundred years long [e.g., Geissman et al. (2010) (Huckleberry Ridge Tuff); Hasegawa et al. (2018) (Kikai-Akahoya tephra); Mochizuki et al. (2022 and in prep) (Shikotsu ignimbrite); Hasegawa et al. (2020) and Gravely et al. (in prep) (Mamaku ignimbrite)]. In the case of Taupō, there exists a clear erosional gap between Y3 and Y4 (see "Eruption products and sequence" section and Fig. 2). Although geological observation concluded that there was no considerable (> years) time gap (Wilson and Walker 1985), no quantitative data, such as a paleomagnetic estimation, have been published.

Using the paleomagnetic method, it is difficult to estimate the longest duration because secular variation can generally return to a similar direction after irregular and indeterminate intervals of time. To estimate the shortest duration, we assumed the fastest changing rate of the PSVC. The fastest rate of change, calculated in 50 year-windows over the past 2000 years from New Zealand is 0.18°/year in declination and 0.09°/year in inclination (Turner et al. 2015a). The shortest duration (time) can be calculated by dividing an angular difference by the fastest rate of change. In this calculation, we took the mean directions from Y1 and Y4-lower units, the difference between which is the largest among the Taupō eruption sequence. Although the angular distance is calculated as 3.4°, the directions of Y1 and Y4-lower are indistinguishable from each other considering their α_{95} values (Table 1, Fig. 7). For a simple quantitative estimate however, we used the differences in declination and inclination between the two units (Y1 and Y4-lower) as follows: $|3.9°–7.1°| = 3.2°$ and $|-53.4°–56.2°| = 2.8°$, respectively. Then, 95% confidence limits in the declination and inclination differences were determined as $\pm 7.6°$ and $\pm 4.4°$, respectively, based on the method of error analysis (Demarest 1983). To generate a difference of $3.2° \pm 7.6°$ in declination, it takes 17.8 ± 42.2 years assuming the fastest changing rate of 0.18°/year. Similarly, the shortest duration calculated from the inclination difference, $2.8° \pm 4.4°$, is estimated as 31.1 ± 48.9 years. As mentioned above, because the angular difference is smaller than the uncertainty, the estimate of duration may be attributed as "zero", or little to no discernable time interval between Y1 and Y4-lower. If focusing on only angular difference without uncertainty, the duration of the Taupō eruption can be estimated to be several tens of years. In this instance, our results are consistent with qualitative geological observations and estimations of the eruption duration (see "Eruption products and sequence" section). Although there is a clear erosional surface between Y3 and Y4, the formation of this surface following the deposition of Y3 may have occurred too quickly to be detected by the paleomagnetic method. However, if the time break between Y3 and Y4 was on the order of several decades to a hundred years, we are confident that the difference in paleomagnetic directions in our data would have provided quantitative evidence for this (cf. Hasegawa et al. 2020; Gravley et al. in prep; Mochizuki et al. in prep).

Paleomagnetic control of the age of Taupō eruption

Finally, paleomagnetic dating was conducted by comparing the overall mean ChRM direction of the deposits to the available paleosecular variation curve (PSVC) for New Zealand using the MATLAB based dating tool of Pavón-Carrasco et al. (2011). The method provides a calculation tool for paleomagnetic dating purposes based on the combination of temporal probability density functions of two or three of the geomagnetic field elements-declination, inclination and intensity. It takes into consideration the uncertainties of the discrete declination and inclination records and those of the secular variation curve.

In this paper, we used the latest PSVC directional record for New Zealand (NZPSV10k; Turner et al. 2015b) which has been updated with recently published radiometric ages and volcanic data in New Zealand. NZPSV10k is compiled from paleomagnetic data from ten sediment cores from three lakes, each independently dated using a combination of radiocarbon dating of included organic material and tephra correlation. NZPSV10k is presented for a latitude of 40 °S and a longitude of 175 °E. To compare a paleomagnetic direction from other locations with NZPSV10k it is necessary to "relocate" it to 40 °S, 175 °E, to compensate for the geographical variation in field, particularly the latitudinal variation due to its dominant geocentric axial dipole component. This is most commonly done by a "virtual geomagnetic dipole relocation". This entails calculating the orientation and/or strength of the geocentric dipole that would produce the observation, then calculating the direction and/or intensity of the field this dipole would yield at the reference location, in this case 40°S, 175°E.

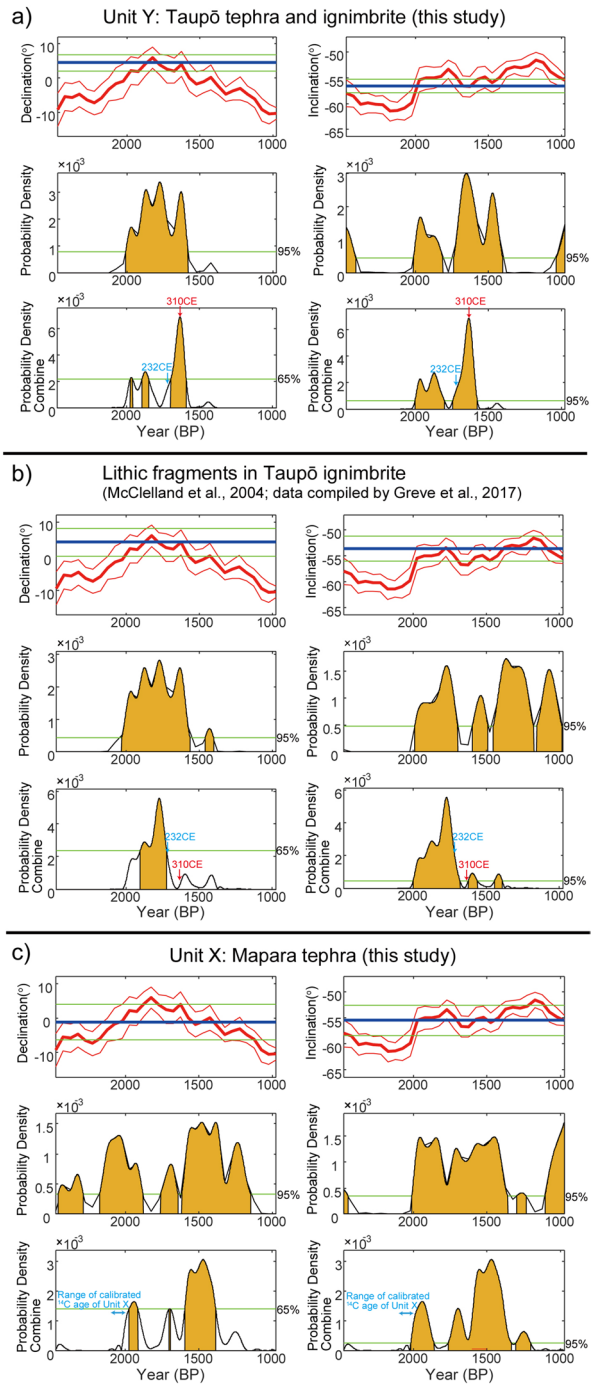

Fig. 10 Results of paleomagnetic dating based on Pavón-Carrasco et al. (2011), and the paleosecular variation curve (PSVC) reference model (NZPSV10k by Turner et al. 2015b). PSVC for the declination, inclination are shown as thick red lines (thin red lines for the associated α_{95}% level), together with the probability density curves (in orange-shade below each PSVC). Paleomagnetic declination, inclinations of our samples (re-located: see text in detail) are shown in the PSVC graphs as blue straight lines; the green dashed lines above and below are the associated α_{95}% levels. The final combined probability density curves are shown in blue-shade (the 65% and 95% confidence levels are shown as a green line, respectively). **a** Taupō sequence (air falls and ignimbrite of Unit Y) (this study), **b** lithic fragments in Taupō ignimbrite (McClelland et al. 2004; data compiled by Greve and Turner 2017), **c** Mapara tephra (Unit X) (this study)

Numerical experiments show that this approach is reliable to better than 0.1°/100 km over the extent of New Zealand.

Correlation of the declination and inclination of our overall mean direction (Dec = 4.3°, Inc = −55.3°, α_{95} = 1.3°, N = 38) after relocation to 40°S, 175°E, as shown in Fig. 10a, yields a probability density function (95% confidence) with two matching age ranges: 2007 BP–1779 BP (57 BCE–171 CE) peaking at 1980 BP and 1870 BP (30 BCE and 120 CE), and 1748 BP–1576 BP (202 CE–374 CE) peaking at 1640 BP (310 CE) (Table 2 and Fig. 10a). The younger of the matched age ranges encompasses the wiggle matched date of 232 ± 10 CE of Hogg et al. (2012). It also extends to younger ages, and in fact peaks at 310 CE, close to the highest probability peak and generalized linear model fit of calibrated ^{14}C ages on samples from distal areas (> 60 km) from the vent(s) of the Taupō eruption presented by Holdaway et al. (2018, 2019). Holdaway et al. (2018, 2019) emphasize the possibility that magmatic (^{14}C-depleted) carbon dioxide (degassed from groundwater) at proximal areas might bias the wiggle-match age of Hogg et al. (2012, 2019), while Hogg et al. (2019) do not accept the suggestion due to unlikeliness of such contamination from groundwater at the sampling site of the wiggle-matched date. The probability density field of our paleomagnetic dating with 65% confidence excludes 232 ± 10 CE (Fig. 10a), and the 310 CE is more consistent with the suggested age by Holdaway et al. (2018)—a Taupō eruption that occurred decades to a century after 232 CE. Interestingly however, the shallower inclination of the direction calculated by Greve et al. (2017) from the lithic fragment data of McClelland et al. (2004), shifts the paleomagnetic age match back to 50 CE–270 CE, with only very minor peaks at later dates (Fig. 10b). Only ages between 50 BCE and 148 CE or between 205 CE–270 CE are consistent with both at the 95% level of confidence.

In addition, we calculated the age of unit X by the same method. The unit X (Mapara tephra) is stratigraphically lower than unit Y (Taupō tephra), and the ^{14}C date can be recalculated as ca. 2100–2000 BP (calibrated by OxCal 4.4 based on SHCal20 curve from the average ^{14}C age of 2160 ± 25 given by Froggatt and Lowe 1990). Our paleomagnetic dating yields matching age ranges between 2028 and 1850 BP (95% probability) or between 2000 and

Table 2 Summary of paleomagneti age estimation

Unit	Dec	Inc	α_{95}	BP	BCE/CE
Unit Y	4.3	−55.3	1.3	2003–1802 or 1745–1577	*53 BCE–148 CE* or **205 CE–373 CE**
*	*4.45*	*−56.58*	*1.3*		
Lithic fragments	*3.9*	−52.2	2.4	2000–1680	**50 BCE–270 CE**
*	*4.11*	*−53.57*	*2.4*	(or 1623–1560 or 1443–1390)	*(or 327 CE–390 CE or 505 CE–560 CE)*
Unit X	358.8	−54.3	2.9	2020–1859	**70 BCE–91 CE**
*	*358.87*	*−55.48*	*2.9*	(or 1768–1202)	*or 182 BCE–748 CE*

* Dec and Inc relocated to 40S, 175E (in italics)

Preferred palaeomagnetic age estimates in bold, other matches in italics

1900 BP (65% probability), as well as a younger match which is unfeasible on stratigraphic grounds (Fig. 10c). The paleomagnetic age of Mapara tephra (unit X) overlaps the probability peak of the calibrated ^{14}C dates at ca. 2000 BP, but also admits younger ages. Our data do not reject either the wiggle matched date of 232 CE for the Taupo eruption (unit Y) or the published age of the Mapara tephra (unit X) but there remains the possibility of biased ^{14}C dates due to magmatic carbon flux in this area, especially in young samples. A more detailed, higher resolution investigation is required to unambiguously resolve the issue.

Conclusion

This study is the first that reports paleomagnetic data acquired for the entire Taupō eruption sequence. It aims to provide further constraints on the eruption age and duration of the Taupō eruption, using paleomagnetic techniques. Key conclusions are:

1. Reliable paleomagnetic data can be obtained from soft and thin tephra layers sampled using a specialized oriented cubing tool. The cube sample should be taken from the fine ash parts of pyroclastic layers without lapilli sized grains.
2. Air fall units record remanent magnetic directions at the time of deposition. Although the magnetization process might be depositional, the direction is consistent with that of co-eruptive ignimbrite, which retains a thermoremanent magnetization.
3. The overall mean paleomagnetic direction of the Taupō eruption sequence obtained in this study is Dec = 4.3°, Inc = −55.3° with 95% confidence of 1.3°. This direction is consistent with the published mean calculated for lithic fragments emplaced within the Taupō ignimbrite (McClelland et al 2004; Greve and Turner 2017).
4. Our best mean paleomagnetic directions between the individual eruptive units differ by no more than 4.1° in declination and 2.8° in inclination. Assuming that all deposits were magnetized during or immediately following their emplacement, these results indicate that the entire eruption occurred over a timeframe less than a few decades. This result supports geological observations (Wilson and Walker 1985; Smith and Houghton 1995a, b), which indicate that the entire eruption sequence was deposited in a matter of days to weeks or possibly months.
5. Paleomagnetic dating was carried out by correlating declination and inclination records, and their associated errors with the latest secular variation curve NZPSV10k of (Turner et al 2015b). At the 95% confidence level, our proposed age band (205 CE–373 CE) encompasses Hogg et al. (2012) original radiocarbon age of 232 CE as well as the proposed younger age around 310 CE (Holdaway et al. 2018, 2019). The probability density function peaks at ~ 310 CE, which coincides with the proposed radiocarbon age of Holdaway et al (2018, 2019). Hence although neither age estimate can be excluded the results support a hypothesis that the Taupo eruption may have occurred decades to a century earlier than originally thought.

Paleomagnetic studies are usually conducted on lava flows or welded tuffs, but here we provide a method that can expand such paleomagnetic studies to evaluate the duration and mode of emplacement and the absolute age of tephra that is not deposited under hot conditions where thermoremanent magnetization occurs. In addition, characterizing and calculating remanent magnetization of ash fall deposits, such as the many layers of the Taupō eruption sequence, opens up further possibilities for correlating more globally distributed tephra, including those found in marine and ice cores.

Supplementary Information

The online version contains supplementary material available at https://doi.org/10.1186/s40623-023-01779-7.

Additional file 1: Table S1. Paleomagnetic data for each sample (cube). Samples showing large MAD values (>10°: Italic) were rejected for the calculation of Unit (site) mean directions (see main text).

Additional file 2: Figure S1. Temperature profiles in the Taupō Ignimbrite and underlying non-welded tephra substrate, calculated using the conductive cooling model of Lerner et al (2019), with a 2 m ignimbrite thickness, initial ignimbrite temperature of 400°C, initial substrate and ambient temperatures of 20°C, and thermal diffusivity of both ignimbrite and substrate = 4.33 × 10 m /s. The number of days after ignimbrite emplacement are noted on the temperature profiles. Unit Y4 is taken to be between 1 and 2 meters below the base of the ignimbrite. The top and base of unit Y4 reach maximum temperatures of ~100°C and ~60°C, about 30 and 60 days after emplacement respectively.

Acknowledgements
We wish to express our gratitude to the editor of EPS and two reviewers.

Author contributions
TH, AG and DG wrote the manuscript. TH, DG, CK, YK, SK and MO participated in the field survey and sampling. TH, CK and YK performed all magnetic experiments and measurements. SS carried out grain size analysis. All authors participated in the interpretation and discussion of the results. All authors read and approved the final manuscript.

Funding
This research was partly supported by the Nuclear Regulation Authority, Japan and JSPS KAKENHI Grant Nos. JP16K01311, JP16KK0092, JP17K05683 (Takeshi Hasegawa).

Availability of data and materials
The datasets used and/or analyzed during the current study are available from the corresponding author on reasonable request.

Declarations

Competing interests
Author SK is employed by Horizons Regional Council. The remaining authors declare that the research was conducted in the absence of any commercial or financial relationships that could be construed as a potential conflict of interest.

Author details
[1]Department of Earth Sciences, College of Science, Ibaraki University, 2-1-1, Bunkyo, Mito 310-8512, Japan. [2]Paleomagnetic Laboratory 'Fort Hoofddijk', Department of Earth Sciences, Utrecht University, Budepestlaan 17, 3584 CD Utrecht, The Netherlands. [3]School of Earth and Environment, University of Canterbury, Private Bag 4800, Christchurch 8140, New Zealand. [4]Massey University, Private Bag 11-222, Palmerston North 4442, New Zealand. [5]Present Address: Horizons Regional Council, 15 Victoria Avenue, Palmerston North Central, Palmerston North 4410, New Zealand. [6]Department of Earth and Environmental Science, Faculty of Advanced Science and Technology, Kumamoto University, Kumamoto 860-8555, Japan. [7]School of Chemical and Physical Sciences, Victoria University of Wellington, P.O. Box 600, Wellington 6140, New Zealand.

Received: 3 August 2022 Accepted: 26 January 2023
Published online: 16 February 2023

References

Baer EM, Fisher RV, Fuller M, Valentine G (1997) Turbulent transport and deposition of the Ito pyroclastic flow; determinations using anisotropy of magnetic susceptibility. J Geophys Res 102:22565–22586. https://doi.org/10.1029/96JB01277
Böhnel H, Pavón-Carrasco FJ, Sieron K, Mahgoub AN (2016) Palaeomagnetic dating of two recent lava flows from Ceboruco volcano, western Mexico. Geophys J Int 207:1203–1215. https://doi.org/10.1093/gji/ggw310
Borradaile GJ, Werner T, Lagroix F (1999) Magnetic fabrics and anisotropy-controlled thrusting in the Kapuskasing Structural Zone, Canada. Tectonophysics 302:241–256. https://doi.org/10.1016/S0040-1951(98)00292-3
de Groot LV, Dekkers MJ, Visscher M, ter Maat GW (2014) Magnetic properties and paleointensities as function of depth in a Hawaiian lava flow. Geochem Geophys Geosyst 15:1096–1112. https://doi.org/10.1002/2013GC005094
Demarest HH (1983) Error analysis for the determination of tectonic rotation from paleomagnetic data. J Geophys Res 88:4321–4328. https://doi.org/10.1029/JB088iB05p04321
Fisher RA (1953) Dispersion on a sphere. Proc R Soc Lond 217:295–305. https://doi.org/10.1098/rspa.1953.0064
Fisher RV, Orsi G, Ort M, Heiken G (1993) Mobility of a large-volume pyroclastic flow—emplacement of the Campanian Ignimbrite, Italy. J Volcanol Geotherm Res 56:205–220. https://doi.org/10.1016/0377-0273(93)90017-L
Foggatt PC, Lowe DJ (1990) A review of late Quaternary silicic and some other tephra formations from New Zealand: their stratigraphy, nomenclature, distribution, volume, and age. N Z J Geol Geophys 33:89–109. https://doi.org/10.1080/00288306.1990.10427576
Folk RL, Ward WC (1957) Brazos river bar; a study in the significance of grain size parameters. J Sedim Res 27:3–26. https://doi.org/10.1306/74D70646-2B21-11D7-8648000102C1865D
Fujii J, Nakajima T, Kamata H (2001) Paleomagnetic directions of the Aso pyroclastic-flow and the Aso-4 co-ignimbrite ash-fall deposits in Japan. Earth, Planet, and Space 53:1137–1150. https://doi.org/10.1186/BF03352409
Geissman JW, Holm D, Harlan SS, Embree GF (2010) Rapid, high-temperature formation of large-scale rheomorphic structures in the 2.06 Ma Huckleberry Ridge Tuff, Idaho, USA. Geology 38:263–266. https://doi.org/10.1130/G30492.1
Greve A, Turner GM (2017) New and revised palaeomagnetic secular variation records from post-glacial volcanic materials in New Zealand. Phys Earth Planet Inter 269:1–17. https://doi.org/10.1016/j.pepi.2017.05.009
Hamilton N, Rees AI (1970) The use of magnetic fabric in paleocurrent estimation. In: Runcorn SK (ed) Paleogeophysics. Academic Press, London, pp 445–464
Hasegawa T, Mochizuki N, Oiwane H (2018) Methods of estimating the durations of super large eruptions based on pyroclastic deposits. J Geogr (chigaku Zasshi) 127:273–288. https://doi.org/10.5026/jgeography.127.273
Hasegawa T, Mochizuki N, Gravley DM, Kusu C, Okada M, Geshi N, Kosik S, Shibata S, Kaenda Y (2020) Evaluation on the durations of large-scale caldera-forming eruptions based on paleomagnetic method: examples from Aira caldera, Japan and Mamaku/Ohakuri Ignimbrites, New Zealand. In: JpGU-AGU joint meeting 2020
Hayashida A, Kamata H, Danhara T (1996) Correlation of widespread tephra deposits based on paleomagnetic directions: link between a volcanic field and sedimentary sequences in Japan. Quat Int 34–36:89–98. https://doi.org/10.1016/1040-6182(95)00072-0
Hogg A, Lowe DJ, Palmer J, Boswijk G, Bronk Ramsey C (2012) Revised calendar date for the Taupo eruption derived by ^{14}C wiggle-matching using a New Zealand kauri ^{14}C calibration data set. Holocene 22:439–449. https://doi.org/10.1177/0959683611425551
Hogg AG, Wilson CJN, Lowe DJ, Turney CSM, White P, Lorrey AM, Manning SW, Palmer JG, Bury S, Brown J, Southon J, Petchey F (2019) Wiggle-match radiocarbon dating of the Taupo eruption. Nat Commun 10:4669. https://doi.org/10.1038/s41467-019-12532-8
Holdaway RN, Duffy B, Kennedy B (2018) Evidence for magmatic carbon bias in 14C dating of the Taupo and other major eruptions. Nat Commun 9:4110. https://doi.org/10.1038/s41467-018-06357-0
Holdaway RN, Duffy B, Kennedy B (2019) Reply to "Wiggle-match radiocarbon dating of the Taupo eruption." Nat Commun 10:4668
Houghton BF, Wilson CJN, McWilliams MO, Lanphere MA, Weaver SD, Briggs RM, Pringle MS (1995) Chronology and dynamics of a large silicic magmatic system: Central Taupo Volcanic Zone, New Zealand. Geology 23:13–16. https://doi.org/10.1130/0091-7613(1995)023%3c0013:CADOAL%3e2.3.CO;2

Houghton BF, Carey RJ, Rosenberg MD (2014) The 1800a Taupo eruption: "Ill wind" blows the ultraplinian type event down to Plinian. Geology 42:459–461. https://doi.org/10.1130/G35400.1
Jelínek V (1981) Characterization of the magnetic fabrics of rocks. Tectonophysics 79:63–67. https://doi.org/10.1016/0040-1951(81)90110-4
Kamata H, Suzuki-Kamata K, Bacon CR (1993) Deformation of the wineglass welded tuff and the timing of caldera collapse at Crater Lake, Oregon. J Volcanol Geotherm Res 56:253–265. https://doi.org/10.1016/0377-0273(93)90019-N
Keating GN (2005) The role of water in cooling ignimbrites. J Volcanol Geothermal Res 142:145–171. https://doi.org/10.1016/j.volgeores.2004.10.019
Kirschvink JL (1980) The least-squares line and plane and the analysis of palaeomagnetic data. Geophys J Int 62:699–718. https://doi.org/10.1111/j.1365-246X.1980.tb02601.x
Lerner GA, Cronin SJ, Turner GM, Rowe MC (2019) Paleomagnetic determination of the age and properties of the 1780–1800 AD dome effusion/collapse of Mt. Taranaki, New Zealand. Bull Volc 81:15. https://doi.org/10.1007/s00445-019-1275-z
Lowe DJ, de Lange WP (2000) Volcano-meteorological tsunamis, thec. AD 200 Taupo eruption (New Zealand) and the possibility of a global tsunami. Holocene 10:401–407. https://doi.org/10.1191/095968300670392643
Lowe DJ, Pittari A (2021) The Taupō eruption sequence of AD 232 ± 10 in Aotearoa New Zealand: a retrospection. J Geogr (chigaku Zasshi) 130:117–141
MacDonald WD, Palmer HC (1990) Flow directions in ash-flow tuffs: a comparison of geological and magnetic susceptibility measurements, Tshirege member (upper Bandelier Tuff), Valles caldera, New Mexico, USA. Bull Volcanol 53:45–59. https://doi.org/10.1007/BF00680319
McClelland E, Wilson CJN, Bardot L (2004) Palaeotemperature determinations for the 1.8-ka Taupo ignimbrite, New Zealand, and implications for the emplacement history of a high-velocity pyroclastic flow. Bull Volcanol 66:492–513. https://doi.org/10.1007/s00445-003-0335-5
Mochizuki M, Hasegawa T, Anai C, Nakagawa M, Shibuya H (2022) Paleomagnetic directional change observed for nonwelded pyroclastic flow deposits of the 46 ka Shikotsu caldera-forming eruption. In: The 152 th SGEPSS general assembly
Ort MH, Orsi G, Pappalardo L, Fisher RV (2003) Anisotropy of magnetic susceptibility studies of depositional processes in the Campanian Ignimbrite, Italy. Bull Volcanol 65:55–72. https://doi.org/10.1007/s00445-002-0241-2
Pavón-Carrasco FJ, Rodríguez-González J, Osete ML, Torta JM (2011) A Matlab tool for archaeomagnetic dating. J Archaeol Sci 38:408–419. https://doi.org/10.1016/j.jas.2010.09.021
Pistolesi M, Rosi M, Malaguti AB, Lucchi F, Tranne CA, Speranza F, Albert PG, Smith VC, Di Roberto A, Billotta E (2021) Chrono-stratigraphy of the youngest (last 1500 years) rhyolitic eruptions of Lipari (Aeolian Islands, Southern Italy) and implications for distal tephra correlations. J Volcanol Geotherm Res 420:1–20. https://doi.org/10.1016/j.jvolgeores.2021.107397
Reynolds RL (1979) Comparison of the TRM of the Yellowstone Group and the DRM of some Pearlette ash beds. J Geophys Res 84:4525–4532. https://doi.org/10.1029/JB084iB09p04525
Smith RT, Houghton BF (1995a) Vent migration and changing eruptive style during the 1800a Taupo eruption: new evidence from the Hatepe and Rotongaio phreatoplinian ashes. Bull Volcanol 57:432–439. https://doi.org/10.1007/BF00300987
Smith RT, Houghton BF (1995b) Delayed deposition of plinian pumice during phreatoplinian volcanism: the 1800-yr-B.P. Taupo eruption. N Z J Volcanol Geotherm Res 67:22l–226. https://doi.org/10.1016/0377-0273(95)00004-E
Taira A, Scholle PA (1979) Deposition of resedimented sandstone beds in the Pico Formation, Ventura Basin, California, as interpreted from magnetic fabric measurements. Geol Soc Am Bull 90:952–962. https://doi.org/10.1130/0016-7606(1979)90%3c952:DORSBI%3e2.0.CO;2
Tarling DH, Hrouda F (1993) The magnetic anisotropy of rocks. Chapman and Hall, London, p 218
Turner GM, Howarth JD, de Gelder GINO, Fitzsimons SJ (2015a) A new high-resolution record of Holocene geomagnetic secular variation from New Zealand. Earth Planet Sci Lett 430:296–307. https://doi.org/10.1016/j.epsl.2015.08.021
Turner G, de Gelder GINO, Howarth J, Greve A, Kinger R, Corkill R, Nilsson A (2015b) NZPSV1k and NZPSV10k: new palaeosecular variation master records for New Zealand: applications for dating and field modeling. In: Abstract/proceedings of the joint assembly (AGU, GAC, MAC, CGU)
Walker GPL (1980) The Taupo pumice: Product of the most powerful known (ultraplinian) eruption? J Volcanol Geotherm Res 8:69–94. https://doi.org/10.1016/0377-0273(80)90008-6
Walker GPL (1981b) The Waimihia and Hatepe plinian deposits from the rhyolitic Taupo Volcanic Centre. N Z J Geol Geophys 24:305–324. https://doi.org/10.1080/00288306.1981.10422722
Walker GPL (1981c) Characteristics of two phreatoplinian ashes, and their water-flushed origin. J Volcanol Geotherm Res 9:395–407. https://doi.org/10.1016/0377-0273(81)90046-9
Walker GPL (1981a) New Zealand case histories of pyroclastic studies. In: Self S, Sparks RSJ (eds) Tephra studies. Reidel, Dordrecht, pp 317–330. https://doi.org/10.1007/978-94-009-8537-7_19
Wilson CJN (1985) The Taupo eruption, New Zealand. II. The Taupo ignimbrite. Philos Trans R Soc Lond 314:229–310. https://doi.org/10.1098/rsta.1985.0020
Wilson CJN (1993) Stratigraphy, chronology, styles and dynamics of late Quaternary eruptions from Taupo volcano, New Zealand. Philos Trans R Soc Lond 343:205–306. https://doi.org/10.1098/rsta.1993.0050
Wilson CJN, Walker GPL (1985) The Taupo eruption, New Zealand I. General aspects. Philos Trans R Soc Lond 314:199–228. https://doi.org/10.1098/rsta.1985.0019
Wilson CJN, Rogan AM, Smith IEM, Northey DJ, Nairn IA, Houghton BF (1984) Caldera volcanoes of the Taupo Volcanic Zone, New Zealand. J Geophys Res Solid Earth 89:8463–8484. https://doi.org/10.1029/JB089iB10p08463
Yukutake T, Sawada M, Yabu T (1964) Magnetization of Ash-fall Tuffs of Oshima Volcano, Izu, I Magnetization of Ash-fall Tuffs. J Geomag Geoelec 16:178–182. https://doi.org/10.5636/jgg.16.178

Publisher's Note